DEVELOPMENT OF AN IMPROVED SEMI-ANALYTICAL MODEL FOR DESCRIBING THE SHEAR STRENGTH OF ROCK JOINT DISCONTINUITIES

M. Jeffery[1,2], L.M. Lapastoure [1], A. Giacomini [1], S. Fityus [1], O. Buzzi [1]

[1] *Priority Research Centre for Geotechnical Science and Engineering, University of Newcastle, Callaghan, 2208, NSW, Australia.*

[2] *michael.jeffery@newcastle.edu.au, +61249218832*

ABSTRACT

The shear strength of rock joints is known to be scale dependent, which is often referred to as the "scale effect". A new method has recently been proposed to solve the long-known issue of scale effect on the shear strength of large discontinuities. This method, stochastic in nature, uses the roughness information available from visible traces to create N synthetic rock surfaces from a rigorous random field model. The shear strength of these N surfaces is then estimated using a semi-analytical model and a distribution of shear strength, with a mean and a standard deviation is produced. This approach was validated at small scale but it was found that the semi-analytical model under-estimates the shear strength at low values of normal stress, which is explained by a number of simplifying assumptions made in regard to asperity shearing. This paper explores strategies to improve the model without compromising its computational efficiency and the resulting improvement in shear strength prediction.

1. INTRODUCTION

Rock instabilities present grave risks to the serviceability of civil infrastructure and mining operations and to human life, especially in coastal and mountain areas. The associated risks and impacts of rock instability has long been acknowledged within the mining industry and by local government authorities who are becoming increasingly aware of their exposure to rock instability-related risks. The prediction of discontinuity shear strength is an important component in large-scale engineering rock mass stability analysis and design applications. However, working directly at large or project scale is not trivial, nor practical. Researchers and engineers tend to employ empirical approaches with inferred parameters or resort to small-scale laboratory sized specimens to predict the shear strength due to the absence of other suitable alternatives. Testing small specimens can be problematic as the results are not directly transferable to a large scale, due to a phenomenon known as the "scale effect" (Barton and Bandis 1980).

The 'scale effect' describes the fact that the shear strength can be dependent on of the size of the specimen tested (Barton and Bandis 1980) and must be accounted for. Thus, to determine the associated full-scale shear strength from a small-scale sample, an additional upscaling step is required to resolve the scale effect. Despite fifty years of progress, leading to significant advancements of knowledge on rock joints and many attempts to address the phenomenon, the scale effect is not fully understood and remains a challenge to resolve. Even though there is a general agreement that scale matters, there is still some uncertainty on how scale affects shear strength. Thus, there is still no consensus on an appropriate method to upscale small specimen test results to a project problem scale.

In recent years, a new approach philosophy has been developed, to resolve the scale effect issue for large scale discontinuities shear strength estimations. Casagrande *et al*. (2018) proposed to shift away from traditional deterministic methods and use rigorous stochastic analyses. The new method uses the roughness information available from visible traces to create a series of synthetic rock surfaces via a random field model. The shear strength of these surfaces is then estimated using a semi-analytical model, from which a distribution of shear strength is obtained, and meaningful design statistics (mean and standard deviation) can be derived. As the approach can be directly applied to large scale discontinuities, thereby using the roughness information available at same scale, it has the potential to minimise or entirely circumvent the scale effect issue (Buzzi & Casagrande 2018).

Casagrande *et al*. (2018) validated the approach at small specimen scale and observed that the semi-analytical model under-estimates the shear strength at low values of normal stress. The authors noted the observed underestimation could be explained by a number of simplifying assumptions made in regards to imposed asperity shearing mechanics.

This paper explores some strategies to improve the shear strength prediction capabilities of the model. Inclined asperity shearing and asperity deformation upon sliding are two recognised mechanistic components of joint shearing but these are not implemented into the original model validated by Casagrande *et al*. (2018). Key subroutines of the shearing mechanics model and it underlying assumptions are revised and expanded to implement these considerations.

Another key element to account for when assessing the predictive capability of a model is the quality and variability of material parameters. Indeed, variability of material strength will affect the shearing behaviour and the shear strength predictions. Several different material strength criteria, derived from the same set of material test data set, were adopted to explore the effects of material strength variability on prediction accuracy.

2. SEMI ANALYTICAL SHEAR STRENGTH MODEL OVERVIEW

The semi analytical model proposed by Casagrande *et al*. (2018), based on the work by Huang, Chang & Chao (2002), estimates the peak shear strength under constant normal stress conditions. The input data are the material strength, a 3D surface (X, Y, Z data) and a shearing direction. The key assumption of the model is that, upon shearing under low confinement stresses, joints dilate by sliding along the steepest asperities. Dilation causes local opening of the joint and a redistribution of the load amongst asperities still in contact. These asperities contribute to the joint shear resistance and are here referred to as 'active facets'. The peak shear strength is sum of the active facets contribution to shear resistance.

This model considers two components of shear resistance: sliding over the asperity and shearing of an asperity along its base referred from here on as 'basal shearing' (refer Figure 1a). In addition, the current model relies on several strong assumptions: clean and matching surface, uniform material strength and rigid rock walls.

The following sections present some of the key components of the model; however, the reader is invited to refer to Casagrande *et al*. (2018) and Buzzi *et al.* (2017) for further information.

2.1 IDENTIFICATION OF ACTIVE FACETS

Once the input surface has been triangulated, the apparent dip (concept proposed by Grasselli 2006) of each triangular facet (β_{app_i}) is calculated as:

$$\beta_{app\_i} = \cos^{-1}(\bar{n}_i . \bar{s}) - 90° \quad (1)$$

where n is the normal unit vector to the facet and s is the unit vector oriented towards the nominated shearing direction. As indicated by Equation 1, the apparent dip depends on the shearing direction.

A variable, called 'critical dip', β^* is used in the process to identify the active facets. The model starts the process using the largest apparent dip, as the initial critical dip. After each iteration, the 'critical dip' is reduced and facets identified with an apparent dip equal or greater than the critical dip are identified to be 'active' are held to be providing to the shear resistance (Casagrande *et al*. 2018). The active facet identification concept is illustrated in Figure 1b. This iterative process is recurring until no more asperity shearing occurs. In this way, all contributing asperities are progressively sheared and so the total of their individual contribution equates to the total shear resistance provided by the joint.

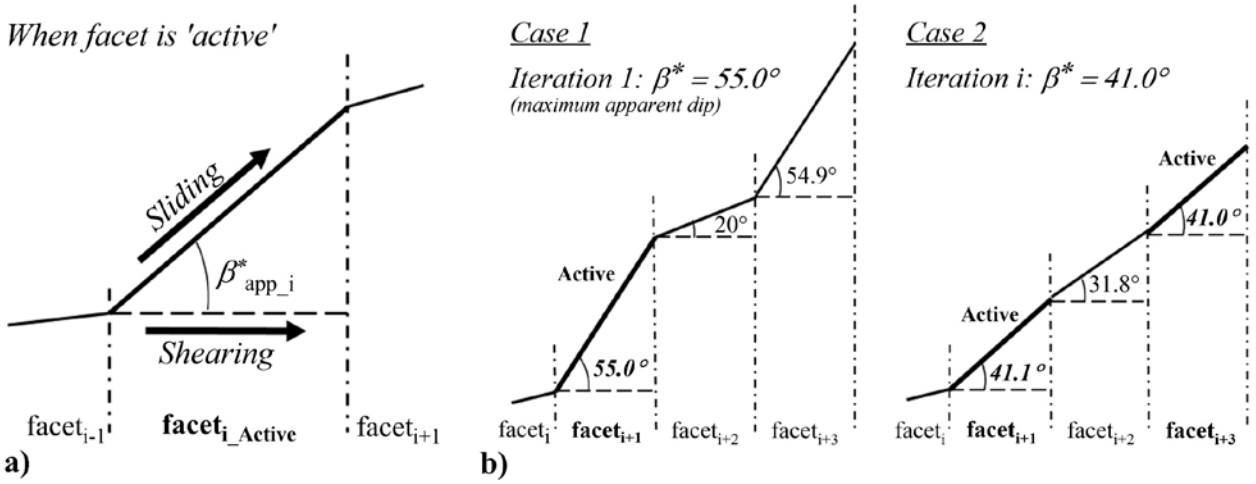

Figure 1: a) Depiction of the two considered shear resistance components for an active facet: sliding over an asperity and shear through the base (basal shearing). b) 2D representation of the active facet identification process: facets are considered active when their apparent dip (β_{appi}) is greater or equal to the critical dip (β^*).

2.2 DETERMINATION OF SLIDING AND SHEARING FORCES

The model assumes an even redistribution of the normal load across the identified active facets that are subjected to a local vertical force, f_{local_i} estimated from Equation 2:

$$f_{local\_i} = \sigma_n . \frac{A_{tot}}{N_{cf}} \tag{2}$$

where A_{tot} is the total area of the discontinuity, N_{cf} is the total number of contributing facets and σ_n is the normal stress applied over whole discontinuity.

Upon shearing, an active facet can sustain a maximum horizontal force, f_{hlocal_i} that is either equal to the force required to slide over facet i ($f_{sliding\_i}$) or shear facet i at its base (f_{shear_i}):

$$f_{sliding\_i} = f_{local\_i} . \tan(\phi_b + \beta_{app\_i}) \tag{3}$$

$$f_{shearing} = A_{ip}(c + \sigma_{local\_i} \tan(\phi)) \tag{4}$$

where f_{local_i} is the applied local vertical force, ϕ_b is the base friction angle of the discontinuity, β_{app_i} is the apparent dip of the facet, A_{ip} is the basal area over which shearing occurs (see Figure 2a), ϕ and c are the equivalent Mohr Coulomb parameters of the intact rock material, back calculated from the Hoek-Brown criterion, via equations 5 and 6:

$$\phi = \sin^{-1} \frac{k-1}{k+1} \tag{5}$$

$$c = \frac{\sigma_{ci}(1 - \sin\phi)}{2\cos\phi} \tag{6}$$

The Hoek-Brown failure criterion is a widely accepted empirical failure criterion for intact rocks and fractured rock masses (Hoek & Brown 1980, Hoek, Carranza-Torres & Corkum 2002). For the intact rock (or mortar in our case), the failure criterion is obtained by fitting the nonlinear empirical equation to triaxial test data, acquired from testing rock specimens.

2.3 PROCESS FOR PREDICTING PEAK SHEAR STRENGTH

For each active facet identified both $f_{sliding\_i}$ and f_{shear_i} are estimated as per Section 2.1, and basal shearing will occur if $f_{sliding\_i} \geq f_{shear\_i}$, otherwise if $f_{sliding\_i} < f_{shear\_i}$, sliding over the facet occurs. The iterations stop when, for a given critical dip, no more shearing occurs and sliding prevails. This idea is illustrated by the convergence of the stress paths in Figure 2b. As shown in Figure 2b, shearing generally prevails over sliding, when the active facets are steep. As the progressive shearing continues, the asperities flatten until a point of convergence, where sliding prevails over shearing. It is at this point, when no other asperities can contribute to the shearing resistance, the process stops and the peak shear stress is computed as per Equation 7.

$$\tau_{p-predicted} = \frac{f_{peak}}{A_{tot}} = \frac{\sum_{i=1}^{N_{af}} f_{local\_i} . \tan(\phi_b + \beta_{app\_i})}{A_{tot}} \tag{7}$$

f_{peak} is the peak shear force, A_{tot} is the total area of the discontinuity, N_{cf} is the total number of active asperities and f_{hlocal_i} is the maximum horizontal force that can be sustained by asperity facet i.

3. OBSERVED UNDERESTIMATION AT LOW NORMAL STRESS

Casagrande and co-workers validated the model on three surfaces of varying roughness; smooth (JRC 2-4), moderately rough (JRC 8-10) and rough (JRC 16-18). The model was validated under six values of normal stress, for multiple shearing directions. Details of the model validation is presented in Casagrande *et al.* (2018) and Buzzi *et al. (*2017). Figure 3a-c presents a comparison of the peak shear strength from the direct shear tests and the semi analytical model.

The authors concluded that the model generally provides a satisfactory estimate of the peak shear strength but a systematic underestimation of shear strength was observed under low normal stress (see Figure 3a-c). Figure 3 also reveals that the magnitude of underestimation at low normal stress values generally increases as the roughness of the surface increases. Buzzi *et al.* (2017), surmised that the source of the underestimation was due to some of the model assumptions or simplified shearing mechanisms considered.

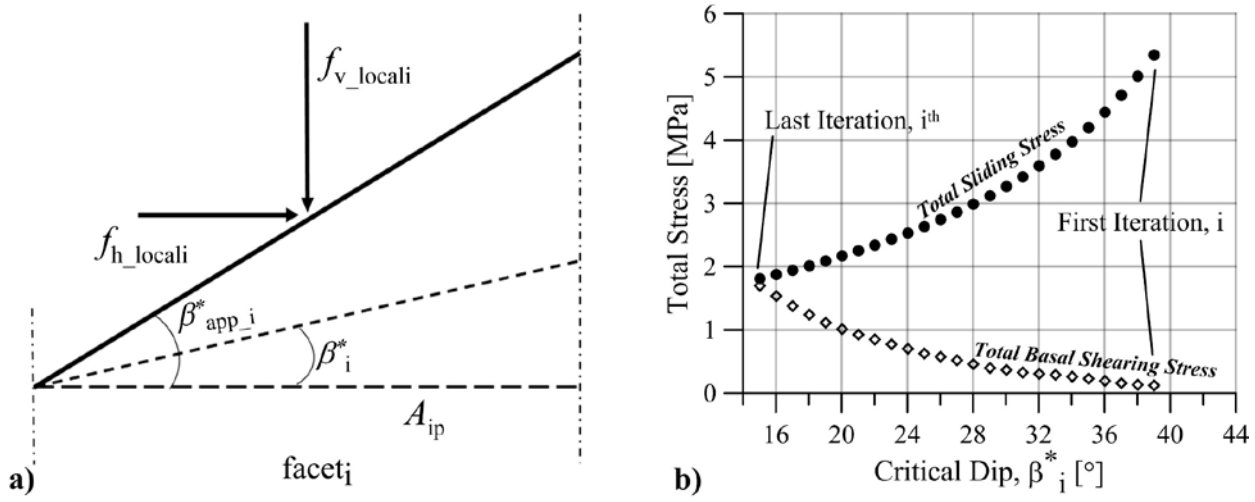

Figure 2: a) 2D representation of an active facet having an apparent dip β_{app_i} and subjected to vertical force f_{local_i} and a horizontal force f_{hlocal_i} (modified after Buzzi *et al.* 2017) b) Convergence of total shearing stress and sliding stress, as a function of critical dip, β* (Note that one marker is plotted every ten values). Surface sheared under a normal stress of 1.5 MPa (adapted from Casagrande *et al*. 2018).

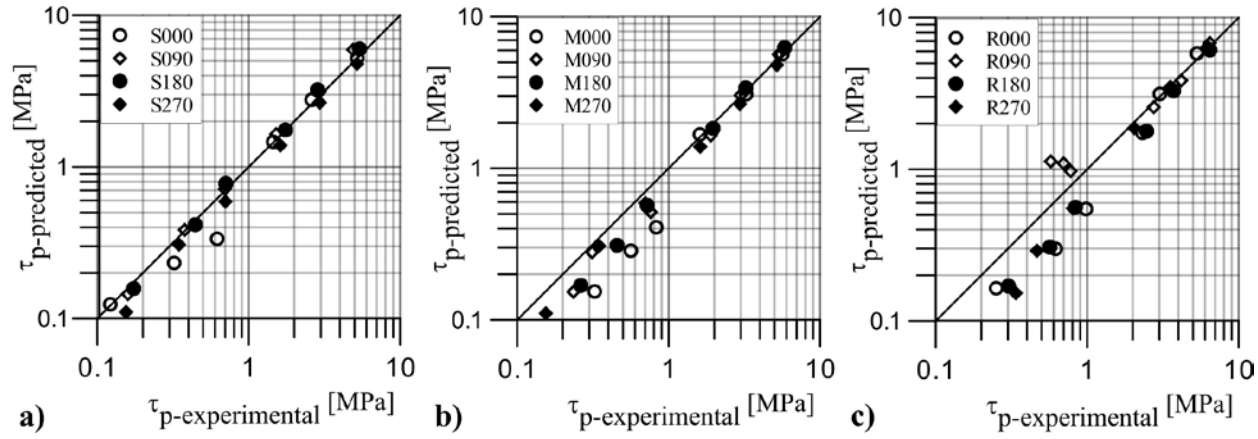

Figure 3: Comparison between experimental and predicted peak shear strength for a) Smooth (S) b) Moderate (M) and c) Rough (R) surfaces (modified after Casagrande *et al*. 2018). The continuous line has a 1:1 gradient.

4. STRATEGIES TO IMPROVE PREDICTIVE CAPABILITIES

This section presents a number of strategies that could help improve the model prediction capabilities, without compromising its computational efficiency. This latter point is paramount as the new approach for shear strength prediction is stochastic in nature and involves a high number of surfaces.

4.1 INCLINED SHEARING THROUGH ASPERITIES

As presented in Section 2.1, occurrence of facet shearing depends on the magnitudes of sliding and shearing forces. In other words, shearing occurs if it takes less force to shear the facet than to slide over it. However, as showed in Equation 4, the shearing force is computed by assuming shearing along the base of the facet, which is not necessarily realistic. Indeed, experimental evidence suggests that shearing might occur along a curve surface and its orientation is a function of the stress level (Seidel & Haberfield 2002). Haberfield and Johnston (1994) also noted that additional inclined shear planes might develop through previously sheared planes, if the shearing resistance exceeds its sliding counterpart.

This section presents the derivation of the local forces accounting for shearing along an inclined plane (referred to as inclined shearing) and its effect on the prediction of shear strength. As the model does not currently capture dilation and displacements, it is assumed that the inclined plane passes through the toe of the facet (see Figure 4a).

Considering local vertical and horizontal forces acting on a facet (f_{v_locali} and f_{h_locali}), Equations 8 and 9 give the expression for the local normal and tangential forces, $f_{n\_locali,}$ and $f_{t\_locali,}$ (see Figure 4a):

$$f_{n\_locali} = f_{h\_locali} \times \sin\beta_i^* + f_{v\_locali} \times \cos\beta_i^* \quad (8)$$

$$f_{t\_locali} = f_{h\_locali} \times \cos\beta_i^* - f_{v\_locali} \times \sin\beta_i^* \quad (9)$$

Furthermore, local normal stress and local tangential stress (respectively the ratio of local normal force and local tangential force over the inclined shear plane area, A^*_i) are related to one another by the Mohr-Coulomb failure criterion (as per Equation 3):

$$\frac{f_{n\_locali}}{A_i^*} = c + \frac{f_{t\_locali}}{A_i^*} \times \tan\phi \quad (10)$$

where c and ϕ are the equivalent Mohr-Coulomb parameters of the intact rock material.

Hence, considering equations 8 to 10, the magnitude of the local horizontal force, $f_{shear\_inclinedi}$, required to facilitate shearing at an inclined plane can be computed as:

$$f_{shear\_inclinedi} = \frac{A_i^*}{\cos\beta_i^* - \sin\beta_i^* \times \tan\phi} \times c + f_{v\_locali} \times \tan(\phi + \beta_i^*) \quad (11)$$

As the horizontal force required to shear along an inclined plane is greater than the force required to shear along the base, it is expected that the sliding and shearing stress will intersect at higher values, resulting in a higher prediction of the peak shear strength as shown in Figure 4b.

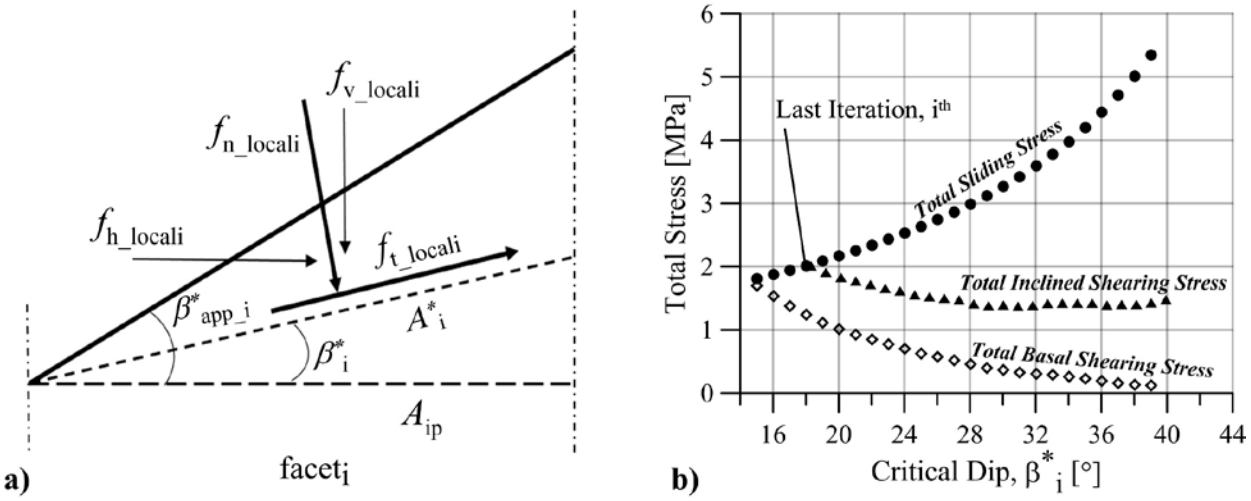

Figure 4: a) 2D representation of an active facet having an apparent dip of β_{appi} , a potential shear plane oriented at β^*_i and subjected to normal force f_{n_locali} and a tangential force f_{t_locali} b) Convergence of total sliding stress, basal shearing stress and inclines shearing stress, as a function of critical dip, β^*_i. (Note that one marker is plotted every ten values). Surface sheared under a normal stress of 1.5 MPa.

4.2 DEFORMATION OF ASPERITIES

The model proposed by Casagrande and co-workers assumes rigid rock wall, which supports the idea that only the steepest asperities remain in contact upon dilation without rotation. However, some rock is not rigid and it is possible for facets to deform under load, which means that some facets that were not initially in contact could come in contact. This would, in turn, affect the redistribution of normal load on the asperities in contact and, possibly, the shear strength (Haberfield & Johnston 1994; Seidel & Haberfield 2002).

The rest of this section outlines the derivation followed to account for elastic deformation of the steepest facets asperities and estimate the force required to slide over facet i, (f_{slide_AD}). Note that subscript "AD" stands for after deformation.

Under the concentration of local normal stress, σ_{n_locali}, a facet inclined at β^*_i will exhibit reduction in the inclination to a new apparent dip, β^*_{iAD} (see Figure 5a). This angular deviation is associated to a local elastic strain, ε_{iAD} that can be estimated by Equation 12 (as a first approximation for a simplified geometry), in terms of the local normal stress and the Young's modulus of the material, E:

$$\varepsilon_{iAD} = \frac{\Delta L_i}{L_i} = 1 - \frac{\tan \beta^*_{iAD}}{\tan \beta^*_i} \simeq \frac{\sigma_{n\_locali}}{E} \tag{12}$$

Note that the actual deformation of a facet for an applied normal stress depends on the interaction with surrounding facets and is a complex phenomenon to model. Equation 10 is a simplified 1D formulation that allows accounting for some degree of deformation without increasing the computational cost of the model. For a given facet, the applied local normal stress is the ratio of the local normal force to inclined facet area A^*_i:

$$\sigma_{n\_locali} = \frac{f_{hAD\_locali} \times \sin \beta^*_i + f_{vAD\_locali} \times \cos \beta^*_i}{A^*_i} \tag{13}$$

In case of sliding, the local vertical force, f_{vAD_locali}, and local horizontal force, f_{hAD_locali}, are linked through the basic friction angle, ϕ_b, and the new reduced apparent dip of the facet, β^*_{iAD} as per Equation 14:

$$f_{hAD\_locali} = f_{vAD\_locali} \times \tan(\phi_b + \beta^*_{iAD}) \tag{14}$$

Finally, considering Equations 12 to 14, the local vertical force required to reduce the apparent dip of a facet can be approximated by:

$$f_{vAD\_locali} \backsimeq \frac{E \times A^*_i \times \left(1 - \frac{\tan \beta^*_{iAD}}{\tan \beta^*_i}\right)}{\cos \beta^*_i + \sin \beta^*_i \times \tan(\phi_b + \beta^*_{iAD})} \tag{15}$$

One key issue with implementing local deformation of the asperities is being able to predict the redistribution of local vertical forces over the joint. This is achieved by an iterative process where the load required to deform all possible active facets (having different apparent dip) to a same dip (referred to as test dip, noted β^*_{iAD}) is computed. All these local forces are added and compared to overall force applied to the joint to achieve a certain normal stress.

If the sum of the local vertical forces is larger than the macro vertical force applied to the whole discontinuity, then the test dip should be increased. In other words, less deformation should take place. In contrast, if the sum of the local vertical forces is lower than the applied force, then the test dip should be decreased, i.e. more deformation should take place. When the correct sliding plane is identified (i.e. when the sum of local forces equates the force applied to the joint), the local horizontal force required to slide over each active facet is computed as per Equation 14.

As previously stated, the deformation of asperities leads to local closure of the joint and a load redistribution, which in turn results in lower estimates of total sliding resistance. As a result, the predicted peak shear strength is expected to be lower than without asperity deformation, especially at high normal stress (1.5 MPa in Figure 5b). Under low normal stress, the effect is only marginal. Although this phenomenon does not directly address the issue of under-estimation of peak shear strength at low normal stress, it is a more realistic mechanism than assuming rigid walls.

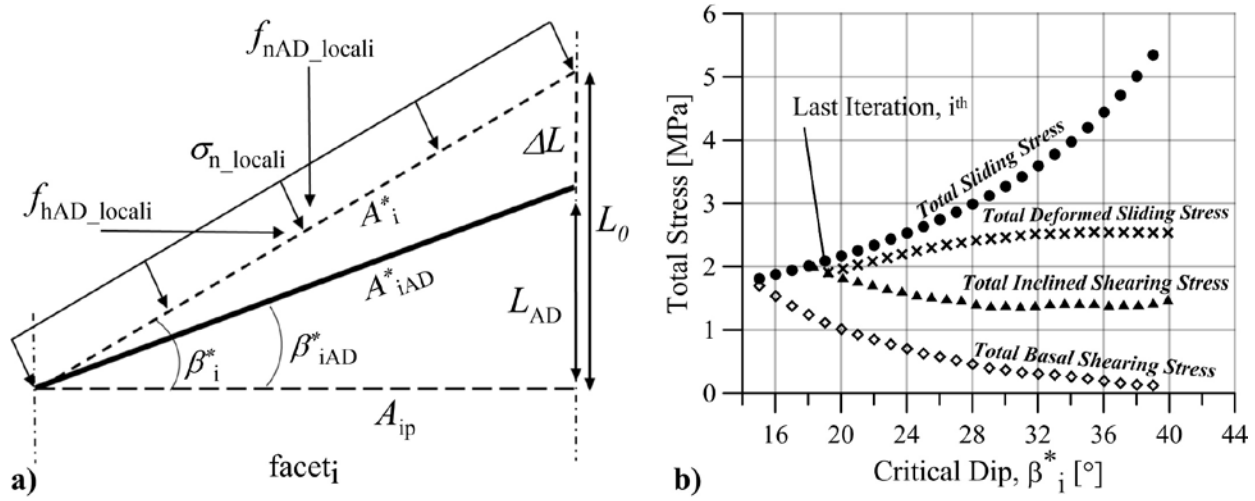

Figure 5: a) 2D representation of a resultant deformed active facet having a dip of β^*_{iAD} and subjected to a redistributed normal force f_{nAD_locali}. b) Comparative convergence of total sliding stress, basal shearing stress, inclined shearing stress and total deformed sliding stress, as a function of critical dip, β^*_i. (Note that one marker is plotted every ten values). Surface sheared under a normal stress of 1.5 MPa.

4.3 EFFECTS OF MATERIAL STRENGTH VARIABILITY

The development of a robust and accurate predictive model requires adequate identification and understanding of all sources of variability. The model proposed by Casagrande *et al.* (2018) requires several inputs including material strength parameters. The introduction of systemic, random and/or gross errors during the material strength characterisation process can lead to variability in the determined material strength parameters and therefore contribute to the uncertainty of the predictions.

Hoek and Brown (1997) noted that the range of minor principal stress values over which a material is tested is critical in determining reliable values for the constants σ_{ci} and mi (uniaxial strength and a fitting constant). Hoek and Brown recommended that a minimum of five tests, equally spaced over a confining stress (minor principal) range of zero to one half of the uniaxial compressive strength, should be conducted. The experimental data used to derive the Hoek-Brown constants reported in Casagrande *et al.* (2018), along with the associated strength envelope (blue line) are presented in Figure 6a. From Figure 6a, it can be seen that the range of confining pressures, over which the tests were undertaken, is quite narrow and well below the recommended range to attain reliable constants. The values of minor principal stress were selected in accordance to the expected normal stresses to be applied to the rock surfaces (up to 1 MPa initially, extended to 6 MPa later). However, with only active facets in contact within the joint, the local stresses are much higher than the range used to characterise the material, which begs the question of the adequacy of any strength criterion fitted using the experimental data showed in Figure 6a. In addition, although mortar is a more controlled material than rock, some variability within batches is possible, as evidenced by the spread of UCS values (from 32 to 47 MPa in Figure 5a). The triaxial compression tests were not repeated, so it is difficult to assess the variability under increasing confining pressure but some can be expected.

To explore the effect of material strength variability on peak shear strength predictions; 4 different failure criteria were considered: the failure criterion established by Casagrande *et al.* (2018) (Hoek-Brown formulation, represented by a blue line and noted CAS), a best-fit of the experimental test data following a Hoek-Brown formulation (noted EBF and shown as the orange line), and two Tresca criteria: an upper bound cohesion (UBC) (purple line) and lower bound cohesion (LBC) (green line). These two can be seen as Hoek-Brown criteria with $m_i = 0$.

The selected failure criteria reflects two distinct behaviours with respect to the initiation and evolution of the cohesive and frictional strength components. Traditional failure criteria such as Hoek-Brown and Mohr-Coulomb assume simultaneous mobilisation and additive of the cohesive and stress dependent frictional strength components. In contrast, the Cohesion Weakening Friction Strengthening (CWFS) model (Hajiabdolmaji, Kaiser & Martin 2002) assumes that the cohesion is first mobilised and as the material is strained, the contribution of frictional resistance increases.

The choice of a cohesion-only criterion, despite appearing to be counter intuitive, is motivated by the fact that some rocks can exhibit CWFS behaviour at relatively low levels of confinement stress. Assuming that the data scattering observed for the UCS also prevails under confinement, it is possible to fit the (few) triaxial data with a Tresca criterion. Note that this is here a sensitivity exercise and does not necessarily represent the most appropriate failure criterion for this material.

The EBF constants were derived via the application of statistical analysis procedure, outlined in Hoek and Brown (1997). The maximum and minimum major principal stresses were adopted as the uniaxial strengths for UBC and LBC respectively. Figure 6 displays the strength envelopes of the selected material parameters in terms of minor and major principal stress (Figure 6a) and normal and tangential stress (Figure 6b). Details of the material parameters used in this study are summarised in in Table 1.

Table 1: Summary of mortar characterisation parameters.

Strength Parameter Set ID	Casagrande *et al.* *(CAS)*	Experimental Best-Fit (*EBF*)	Upper Bound Cohesion (*UBC*)	Lower Bound Cohesion (*LBC*)
Uniaxial Strength, σ_{ci} [MPa]	39.7	38.6	47.8	31.9
Hoek-Brown constant, m_i	35.2	11.9	0.0	0.0
Young's Modulus, E [MPa]	2 950 [A]			
Basic Friction Angle, φ_b [°]	35.3 [B]			

Notes: [A] Derived from the uniaxial compressive strength stress-strain data, obtained during the mortar characterisation phase.
[B] As reported by Casagrande *et al.* (2018).

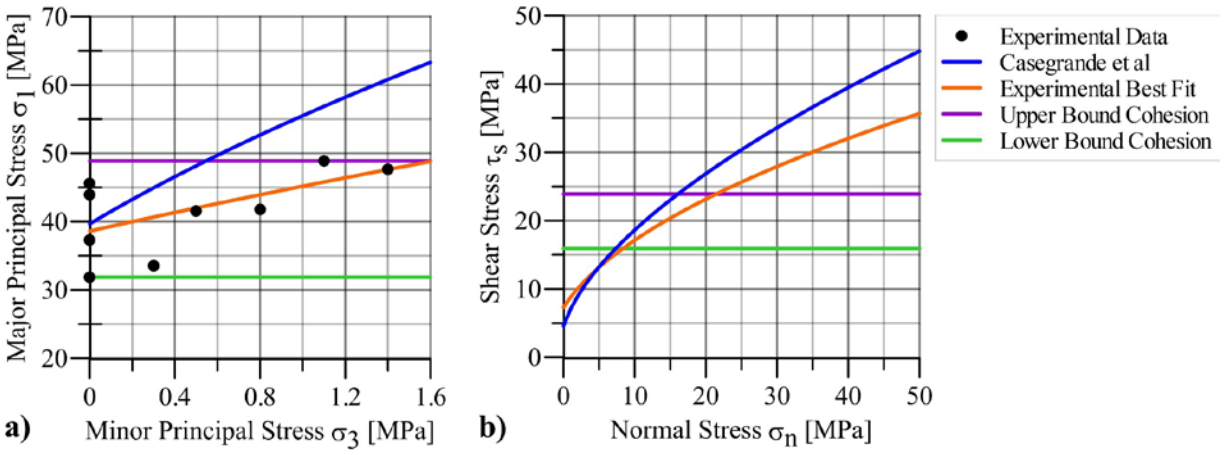

Figure 6: Results of the mortar strength characterisation a) Plot of uniaxial compressive strength and triaxial test data, with projection of potential material strength envelopes b) Strength envelopes plotted in a "shear stress – normal stress" plane over a wider range of normal stress.

5. RESULTS & DISCUSSION

In this section, the results obtained by Casagrande *et al.* (2018) on the three surfaces, under six normal stresses and four shearing directions are compared to the predictions obtained by the new model (with inclined shearing and asperity deformation) using the four material strength parameters of section 4.3.

Figure 7 presents the cumulative distributions of relative error between model prediction and experimental values for all testing combination for each surface. Figures 7a-c focus on the results obtained under low values of normal stress (<0.6 MPa), whereas Figures 7d-f pertain to all values of normal stress (up to 6 MPa). Arbitrary bounds of -20% and +20%, deemed an acceptable target, are also highlighted. Figures 7a to 7c confirm the observation that the original model (black line) leads to some underestimation at low normal stress and that this effect is exacerbated for rougher surfaces.

The effect of revising the model according to sections 4.1 and 4.2, while keeping the same strength parameters, can be assessed by comparing the black line (original model) and blue line (revised model) in Figure 7. Implementing new mechanisms in the model has resulted in higher shear strength predictions and a shift of the distribution to the right. In other words, the problem of under-estimation has changed into a problem of over-estimation, which can be more problematic since it is less conservative. Revising the shear strength parameters, compared to those selected originally by Casagrande *et al.* (2018) partly addresses this issue of overprediction, which is not a surprise considering the failure criteria showed in Figure 6. This, however, shows how critical is the selection of shear strength parameters for the model.

The changes in error distribution presented in Figure 7 suggest that the changes made to the model and considerations about material variability are valid, but require further refinement. It was observed that reduction of underestimation error for M and R surface predictions under low values of normal stress comes at the cost of unavoidable overestimations of S surfaces predictions. The cause of this is currently unknown and needs to be further explored. Ideally, the changes made to the local shearing mechanisms should have different magnitudes at low and high stresses in order to result in a steepening of the error distribution rather than a simple shift.

With respect to reducing the underestimation at low values of normal stress and increasing general accuracy for all values of normal stress, it was determined that the adopted EBF parameters provide the most appropriate error distributions, balancing between underestimating and overestimating predictions, whilst increasing the total proportion of predictions within the bounds. This is somewhat expected as the strength parameters were the 'best fit' and best represent the limited mortar strength characterisation data available.

In light of this conclusion, the experimental shear strength data are now compared to the original predictions (by Casagrande *et al.* (2018) and those obtained from the revised model with the EBF criterion in Figure 8a-c. Visually, the predictions using the revised model and EBF parameters are better than those from the original model. Interestingly, the generally good agreement of the predictions presented in Casagrande *et al.* (2018), were achieved using non representative material parameters and a model that did not consider inclined shearing and asperity deformation. It is possible that the overestimated strength envelope may have compensated for the exclusion of more complicated mechanics.

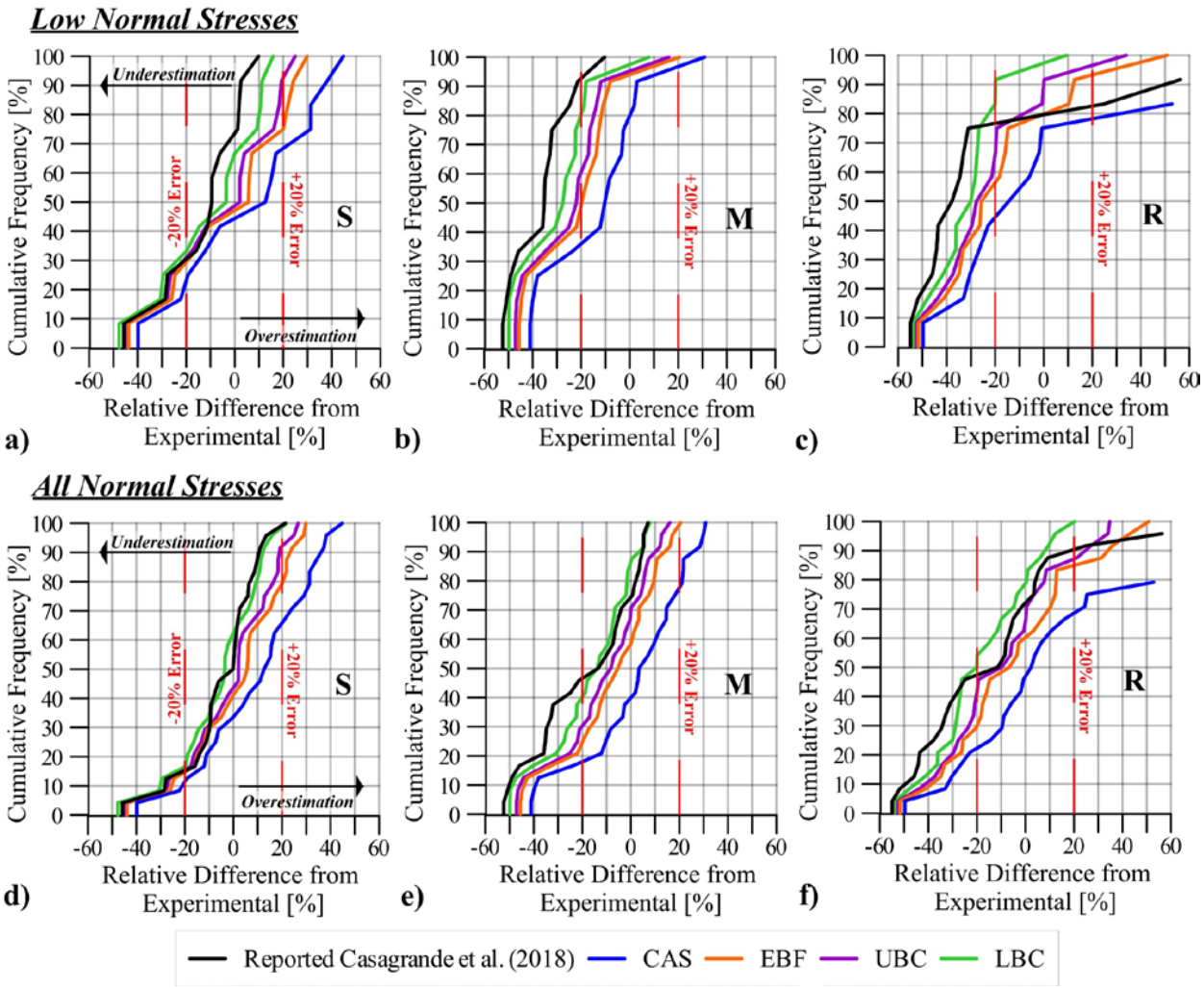

Figure 7: Comparison of cumulative distribution of prediction relative error for all three surfaces (S, M & R), four sets of material parameters and under low normal stresses (<0.6 MPa) (a-c), All normal stresses (d-f) and the associated results reported in Casagrande et al. (2018)

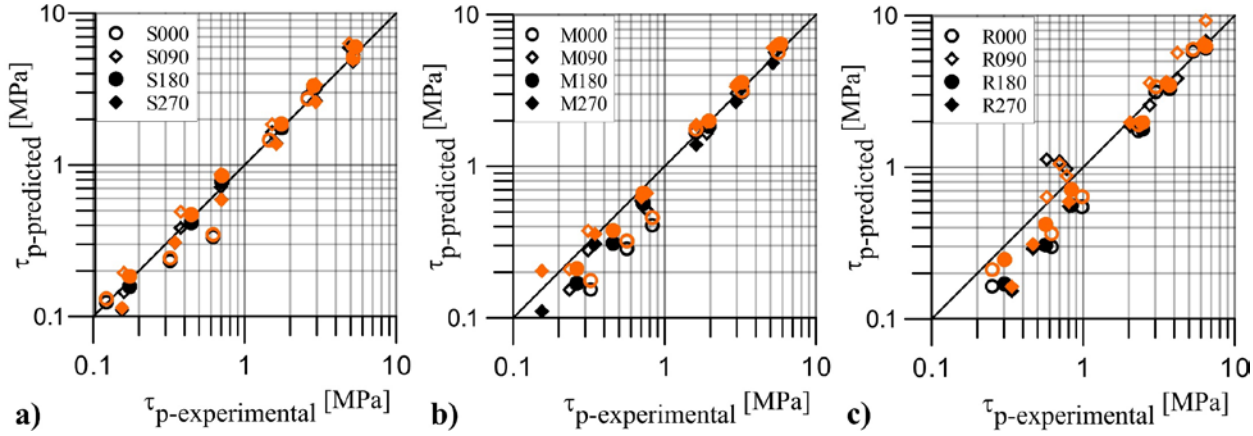

Figure 8: Comparison between experimental and predicted peak shear strength for a) Smooth (S) b) Moderate (M) and c) Rough (R) surfaces (modified after Casagrande *et al.* 2018). Black symbols indicate the results reported by Casagrande *et al.* (2018) and orange symbols denote the results obtained with the refined model and EBF parameters. The continuous line has a 1:1 gradient and the dashed lines indicate ±20% error.

Despite some improvement, not all cases of underprediction and overprediction have been eliminated. Instances of significant underestimations (of up to 60%) reported by Casagrande *et al.* (2018) could not all be resolved using the revised model and the different strength criteria. One possible cause of discrepancy between the model and the experimental data may also lie within the strength variability of the joint replicas tested. Because of a limited number of moulds, only one replica could be casted every day, meaning that each test corresponds to a different batch. Although the procedure to prepare the material and cast the specimens was repeatable, one cannot totally dismiss the possibility of variability from batch to batch. Thus, if the assumed mortar strength represents a weaker mortar mix in comparison to the mix used to cast the joint replicate, the resultant shear strength predictions will produce an underestimating result.

The influence of variability on prediction accuracy is conveyed by the variable nature of relative error distribution profiles presented in Figure 7d-f. From Figure 7d-f, it can be seen that variable material strength parameters can facilitate a wide range of predictions and error. During the course of the study, several sources of variability within the model was identified; variable mortar material strength, provision of a narrow testing stress range and the questionable strength criteria.

The introduction of uncontrolled variability during material characterisation processes reduces the reliability of the model's shear strength predictions. This highlights the importance of rigorous material characterisation for validating, refining and the ongoing use of predictive models. Accurate material characterisation should incorporate sufficient stress ranges and include multiple tests to capture possible material strength variability.

The effect of revising the model according to sections 4.1 and 4.2, with respect to computational efficiency, can be evaluated by comparing the computation times associated to a model incorporating the inclined shearing only (black scatter) and a model incorporating both inclined shearing and wall deformability (blue scatter) in Figure 9. Computation times were obtained for surfaces S, M and R, all consisting around 65,000 facets, under several values of normal stress. The model, implemented in C#, was running on a computer having the specifications: Intel(R) Core(TM) i5-7300U CPU @ 2.60GHz, 8GB of RAM.

Figure 9a shows that the implementation of deformability leads to significant increase in computational time (by an average factor of 15), compared to a model that only contains the revised shearing mechanics. This effect is attributed to the complex iterative process required to redistribute the forces amongst deformed asperities. Note that the wide range of computational times for a given normal stress is related to the wide range of numbers of sheared facets for different surface roughness.

As discussed in the introduction, the model is to be used for analysing large-scale discontinuities in a stochastic manner. Pilkington surface (Buzzi *et al*. 2018) is only 4 m^2 but already contains ~ 8 million facets (100 times more than surfaces S, M and R), which highlights the fact that computational efficiency is critical.

As such, and because of the little effect deformability seems to have on the shear strength prediction (less than 3%, see Figure 9b), it is here proposed to use the model with inclined shearing but no deformability in order to maintain high computational efficiency and being able to apply the new stochastic method to large in situ surfaces.

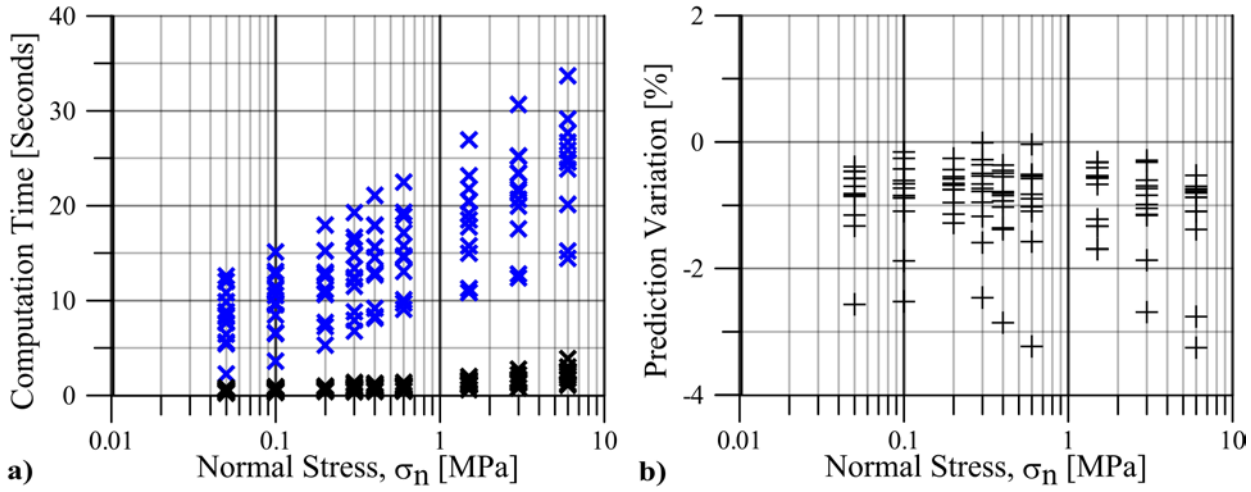

Figure 9: a) Evolution of computational time as a function of the normal stress and implemented improvements. Revised model implementing only the inclined shear revision (black) and both inclined shearing and deformability (blue). b) Scale of peak shear stress prediction variation between revised models as a function of the normal stress.

6. CONCLUSION

This paper presents the steps followed to improve the predictive capability of a shear strength model originally developed by Casagrande *et al*. (2018). The model was developed in the context of a novel approach to predict the shear strength of large in situ discontinuities and it was observed that its simple formulation was computationally efficient but possibly led to systematic under estimation of peak shear strength prediction under low normal stress and for rough surfaces.

The revision of some key shearing mechanisms resulted in better shear strength predictions, in particular at low values of normal stress. However, the results are strongly influenced by the choice of material strength parameters: using reported by Casagrande *et al*. (2018) in the revised model resulted in overestimations of shear strength. In contrast, three other possible criteria led to better predictions. This observation highlights the need to adequately characterise the material and capture the possible material strength variability. Also, the strength testing program devised to characterise the material should reflect the high stress levels within the joint due to stress localisation rather than the overall stress applied to the specimen. The analysis of large discontinuity surfaces requires computationally efficient models. The implemented asperity deformation mechanism greatly reduces computation efficiency, requiring further development and refinement.

7. ACKNOWLEDGEMENTS

The authors acknowledge the financial support provided by Pells Sullivan Meynink, Engineering Consultants, Sydney.

8. REFERENCES

Hajiabdolmajid, V, Kaiser, P, & Martin, C 2002, 'Modelling brittle failure of rock', *International Journal of Rock Mechanics and Mining Sciences*, vol. 39, pp. 731-741, doi:10.1016/S1365-1609(02)00051-5.

Barton, N, & Bandis, S 1980, 'Some effects of scale on the shear strength of joints', *International Journal of Rock Mechanics and Mining Sciences*, vol. 17, no. 1, p. 69-73, doi:10.1016/0148-9062(80)90009-1.

Buzzi, O, Casagrande, D, Giacomini, A, Lambert C, & Fenton G 2017, 'Towards a new approach to avoid the scale effect when predicting the shear strength of large in situ discontinuity', Geo-Ottawa 2017. Paper #161, 8 pages.

Buzzi, O, & Casagrande, D 2018, 'A step towards the end of the scale effect conundrum when predicting the shear strength of large in situ discontinuities', *International Journal of Rock Mechanics and Mining Sciences*, vol. 105, p. 210-219, doi:10.1016/j.ijrmms.2018.01.027.

Casagrande, D, Buzzi, O, Giacomini, A, Lambert, C, & Fenton, G 2018, 'A New Stochastic Approach to Predict Peak and Residual Shear Strength of Natural Rock Discontinuities', *Rock Mechanics and Rock Engineering*, vol. 51, no. 1, p. 69-99, doi:10.1007/s00603-017-1302-3.

Haberfield, C, & Johnston, I 1994, 'A mechanistically-based model for rough rock joints', *International Journal of Rock Mechanics and Mining Sciences*, vol. 31, no. 4, p. 279-292, doi:10.1016/0148-9062(94)90898-2.

Hoek, E, & Brown, E. 1980, 'Underground excavations in rock', The Institution of Mining and Metallurgy, London

Hoek, E, & Brown, E 1997, 'Practical estimates of rock mass strength', *International Journal of Rock Mechanics and Mining Sciences*, vol. 34, no. 8, p. 1165-1186, doi:10.1016/S1365-1609(97)80069-X.

Hoek, E, Carranza-Torres, C, & Corkum, B, 2002, 'Hoek-Brown failure criterion-2002 edition', *Proc. of the 5th North American Rock Mechanics Symposium*, Toronto, p. 267-273.

Huang, T, Chang, C, & Chao, C 2002, 'Experimental and mathematical modelling for fracture of rock joint with regular asperities', *Engineering Fracture Mechanics*, vol. 69, p. 1977-1996, doi:10.1016/S0013-7944(02)00072-3.

Seidel, JP, & Haberfield, CM 2002, 'A theoretical model for rock joints subjected to constant normal stiffness direct shear', *International Journal of Rock Mechanics and Mining Sciences*, vol. 39, no. 5, p. 539-553, doi:10.1016/S1365-1609(02)00056-4.